73rd International Astronautical Congress (IAC), Paris, France, 18-22 September 2022.

IAC-22,A6,6,4,x69631

Dynamic Model and System Design of a 1U CubeSat Drag Sail Module

Luca Diazzi[a]*, Ilaria Ciriolo[a], Franco Bernelli-Zazzera[a], Camilla Colombo[a]

[a] *Department of Aerospace Science and Technology, Politecnico di Milano, Via G. La Masa 34, 20156 Milano, Italy*, luca.diazzi@mail.polimi.it
* Corresponding Author

Abstract

Nowadays, the large number of objects in Low Earth Orbit (LEO) consists of debris, so de-orbiting strategies must be implemented to ensure satellite disposal after its End of Life (EoL). In LEO, the atmospheric drag is the dominant force, so drag sails are used to speed up the satellite re-entry. One issue of such devices is that they largely depend on attitude control. A potential solution is to design the sail as a pyramid to remain possibly aligned with the relative wind direction. The scope of this work is to analyse this geometry and provide a solution to sail storage in a 1U CubeSat module. The first part is dedicated to the implementation of the satellite dynamical model. It is used to simulate the CubeSat orbital and attitude motion during de-orbiting, to numerically prove the stabilization effect of the pyramidal sail, considering the major environmental disturbances acting on the satellite. The second part is devoted to the preliminary design of the module, containing the sail, the stowage and deployment systems.
Keywords: drag sail, debris mitigation, CubeSat

Nomenclature

Variable	Description	SI unit
μ	Earth's gravitational parameter	km^3/s^2
η	Reflectivity	-
γ	Total stability angle	deg
Φ	In plane stability angle	deg
Ψ	Out of plane stability angle	deg
ρ	Density	kg/m^3
A	Area	m^2
$\mathbf{c}$	Normalized position vector	$-$
C_D	Drag coefficient	-
I	Inertia	$kg \cdot m^2$
J_2	Earth's oblateness	-
$\mathbf{n}$	Normal unit vector	-
p_{SRP}	Solar pressure at 1 AU	N/m^2
$\mathbf{r}$	Position vector	km
R	Earth radius	km
$\mathbf{u}$	Velocity unit vector	-
$\mathbf{v}$	Velocity vector	km/s
x, y, z	Coordinates	km

Acronyms/Abbreviations

Acronym	Description
EoL	End of Life
GG	Gravity Gradient
HRM	Hold and Release Mechanism
IADC	Inter-Agency Space Debris Coordination Committee
LEO	Low Earth Orbit
RAAN	Right Ascension of Ascending Node
SRP	Solar Radiation Pressure
TRL	Technology Readiness Level

1. Introduction

Due to the rapid expansion of the space activities, the number of satellites in orbit has increased. The problem of possible collisions is nowadays of major importance since even a single impact can lead to mission failures generating space debris, whose number must be controlled to avoid catastrophic consequences. For this reason, it is fundamental to implement mitigation actions. Moreover, the future LEO population will be dominated by small satellites with limited propulsion capabilities; this leads to the development of passive de-orbit technologies, in which area-augmentation devices play an important role. Since the latter largely depends on attitude control, a potential solution is to design a pyramid sail to keep the satellite aligned with the relative "wind" direction.

The following analysis is focused on a generic 6U CubeSat, where 1U will be dedicated to the drag sail. The implemented dynamical model simulates both the CubeSat orbital and attitude motion during de-orbiting, to numerically prove the pyramidal sail stabilization effect. The model was used to test several initial conditions in terms of orbital parameters, understanding the limits of the sail as passive attitude stabilization and re-entry device. Then a preliminary design has been performed, with the selection of a suitable technology to

fit the payload in 1U, making it independent from the rest of the CubeSat. Finally, the manufacturing process has been investigated to understand the design feasibility.

2. State of the art

According to IADC guidelines [1], satellites in LEO should be de-orbited in 25 years at most, through active or passive strategies: the former use propulsion while the latter take advantage of external perturbation forces. In particular, drag sails can be used as passive de-orbiting devices: they increase the drag surface area, reducing the decay time. A drawback is the great dependency on attitude control. In this case, conventional methods cannot be used [2] because the amount of attitude torque to counteract the SRP can be excessive and propellant-based attitude control systems require a large amount of propellant, limiting the satellite operational lifetime. A potential solution is to use a pyramid-shaped sail, that acts as a passive stabilization device.

From a technological viewpoint, the drag sail module main hardware components are booms, sails and deployment mechanisms. Sails can be rigid and non-rigid, meaning that they, respectively, need or not some kind of supporting structure once deployed [2]. Non-rigid sails show some advantages, but they are too flexible, and this often has deleterious effects on attitude control. Rigid sails maintain their shapes by connecting membrane edges to the booms, which can be composite [3] or inflatable structures [4]. The first one can be flattened and then longitudinally rolled onto a hub; in this way their stowed volume is very limited. The deployment is obtained by unrolling the booms, usually exploiting actuators. During this process, their section changes from a flat configuration to one that depends on the selected geometry. However, they are quite heavy, and their mechanical parts can be a major source of failure. Inflatable space structures are promising candidates, even if the TRL is still low. Some advantages include low volume when stored for launch, low system complexity, and a simple deployment mechanism. Challenges are ground testing, which is complex and costly, and the search for efficient packing schemes. Different storage methods are:

- Coiling and Wrapping: a common stowage method which consists in first flattening the uninflated boom and then rolling it into a coil or wrapping it around a hub;
- Z-folding: in this method the boom is first flattened and later folded back and forth at regularly spaced intervals at discrete lines;
- Origami Folding: it consists of different patterns that allow an extremely compact stored configuration;
- Conical Folding: by introducing a slight taper, a conical boom is formed, providing a compact telescopic stowage configuration.

Drag de-orbit systems have already been used in different past missions and are nowadays of great interest and under constant development.

3. Dynamic model

The satellite geometry has been modelled as a union of two separate parts: the main bus, which is the 6U CubeSat, and the pyramidal sail, responsible for quickening the re-entry and stabilizing the satellite attitude. The geometrical model is shown in Fig. 1.

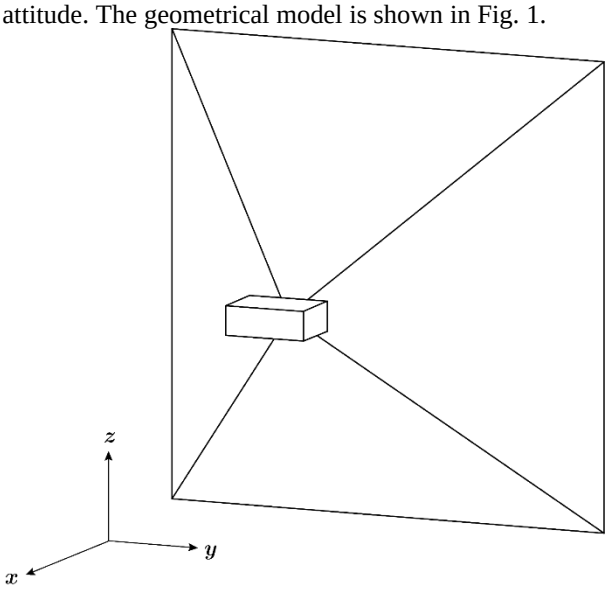

Fig. 1. Representation of the satellite geometry and body axes

The implemented dynamical model considers both orbital and attitude motion of the spacecraft. The orbital dynamics is described with the classical two-body formulation [5], while the attitude dynamics is expressed using the well-known Euler equations and quaternions as kinematic parameters. Since this work wants to investigate the capability of the sail to passively align the x-axis of the body frame to the wind velocity, the dynamical model must include the main perturbing effects typical of the space environment in LEOs. In particular, the modelled disturbances are:

- **Gravitational Effects**, which are due to Earth and CubeSat non-uniform mass distribution. They include the J_2 effect [6], which affects the orbital motion only, and the gravity gradient torque [7], related only to the attitude dynamics. Their expression is, respectively, given as follows:

$$\boldsymbol{a}_{J_2} = -\frac{3\mu J_2 R^2}{2r^5}\begin{bmatrix} x\left(1-\frac{5z^2}{r^2}\right) \\ y\left(1-\frac{5z^2}{r^2}\right) \\ z\left(3-\frac{5z^2}{r^2}\right) \end{bmatrix} \qquad (1)$$

$$\boldsymbol{M}_{GG} = -\frac{3\mu}{R^3}\begin{bmatrix} c_3c_2(I_z - I_y) \\ c_1c_3(I_x - I_z) \\ c_1c_2(I_y - I_x) \end{bmatrix} \quad (2)$$

- **Air Drag**, which is due to residual atmosphere below 1000 km of altitude and is the external action exploited by the sail to accomplish the pointing requirement. It is expressed as follows [7]:
$$\boldsymbol{F} = -\frac{1}{2}\rho C_D v_{rel}^2 A_{exp}(\boldsymbol{n}\cdot\boldsymbol{u}_{rel})\boldsymbol{u}_{rel} \quad (3)$$
where CD is typically considered ≃ 2.5
- **Solar Radiation Pressure**, which is due to the Sun and is particularly relevant due to the large, exposed area of the sail. It must be noticed that the Earth can shadow part of the satellite orbit, making the SRP effect null in those regions. Its formulation is given as [7]:
$$\boldsymbol{F} = -p_{SRP}A_{exp}(\boldsymbol{n}\cdot\boldsymbol{u}_s)(2\eta(\boldsymbol{n}\cdot\boldsymbol{u}_s)\boldsymbol{n} + (1-\eta)\boldsymbol{u}_s) \quad (4)$$
where $0 \leq \eta \leq 1$.

3.1 Satellite self-shadowing

In addition, a deeper analysis regarding the satellite self-shadowing has been carried out, since the computation of the external torque is heavily dependent - due to the sail large dimensions - on the in-light portion of the satellite surfaces. In particular, the surfaces shadows on others can be computed using a customized version of the Z-Buffer algorithm, which is used in computer graphics to render a 3D scene in a 2D image, as shown in Fig. 2. The left part shows the light viewpoint of the scene and the image reconstruction using the data stored in the Z-Buffer. The right part instead shows the rendering of the image from the camera point of view.

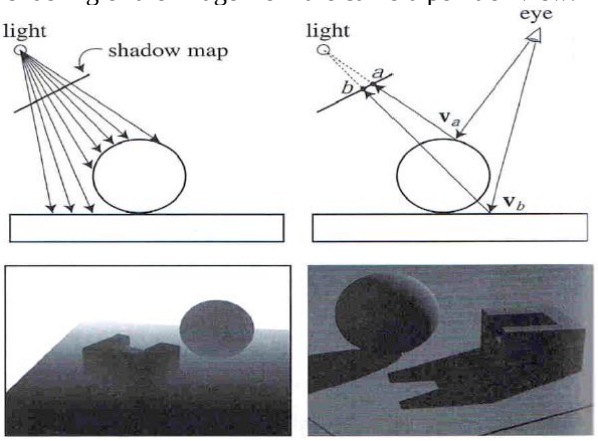

Fig. 2. Shadow mapping.

The basic idea behind the Z-Buffer (and in general the shadow maps) is to render the scene from the light viewpoint and compute the z coordinate of each visible point composing the different surfaces: when two or more of those points fall into the same pixel of the image plane, the one in light is the closest to the light source. The Z-Buffer allows a quite simple implementation and computational efficiency if compared to other rendering or shadowing algorithms, as ray casting, planar shadows, or shadow volumes. The pseudo-code of the implemented algorithm is

1. Initialize depth of each pixel of the scene, i.e. *z(i,j) = Inf*
2. Initialize list of pixel in light, i.e. $inlight_{id}(i,j) = NaN$
3. **for** each polygon in the scene **do**
4. **for** each pixel in the polygon projection **do**
5. Compute the z component of the point *(x,y)* in the polygon, corresponding to pixel *(i,j)*
6. **if** *z < d(i,j)* **then**
7. Update the closer point, i.e. *d(i,j) = z*;
8. Save the closer point, i.e. $inlight_{id}(i,j) = point_{id}$;
9. **end if**
10. **end for**
11. **end for**

Finally, Fig. 3 shows an example of the model above described, applied to the study case. The two figures represent two different views of the same illustrative scene.

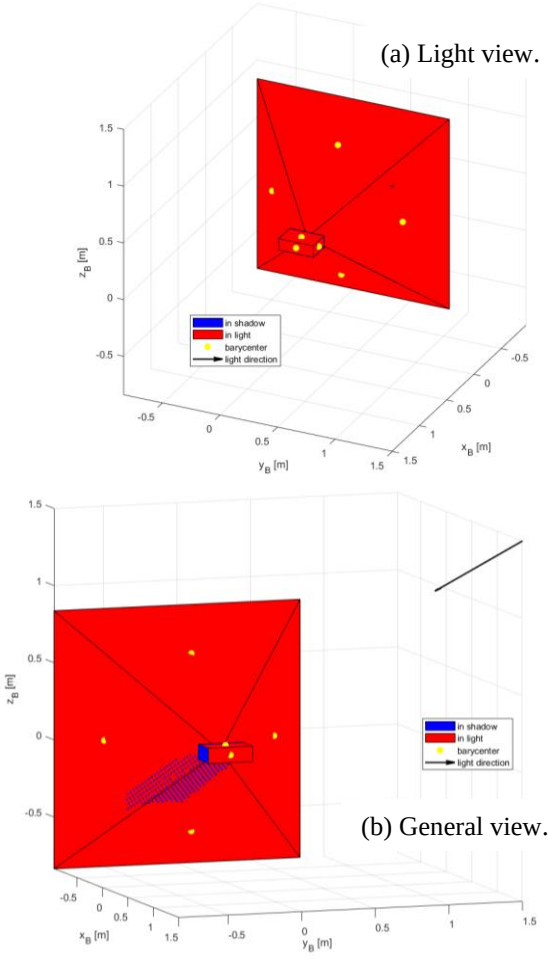

(a) Light view.

(b) General view.

Fig. 3. Example of CubeSat self-shadowing.

Fig. 3a shows the image from the light source point of view, while Fig. 3b is a more general view, used to reveal the shadows of the bus onto the sail. In particular, the blue points represent the discretized pixels composing the sail that are shadowed and the yellow circles the geometrical centre of the non-shadowed area, that represents the force application point.

3.2 Simulations

In order to investigate the effective capability of the pyramidal sail to stabilize the satellite attitude, three angles have been introduced:

1. the angle between the relative wind velocity $\mathbf{u}_{rel}$ and the satellite x-axis $\mathbf{i}_B$, named γ. It is computed as $\gamma = \arccos(\mathbf{i}_B \cdot \mathbf{u}_{rel})$
2. the angle representing the in-plane oscillations of the spacecraft (see Fig. 4), named Φ. It is computed starting from the components of the $\mathbf{u}_{rel}$ unit vector expressed in the body frame as $\Phi = \arctan(\boldsymbol{u}_{rel}^{y} / \boldsymbol{u}_{rel}^{x})$
3. the angle representing the out-of-plane oscillations of the spacecraft (see Fig. 4), named Ψ. It is computed starting from the components of the urel unit vector expressed in body frame as $\Psi = \arcsin(\boldsymbol{u}_{rel}^{z})$

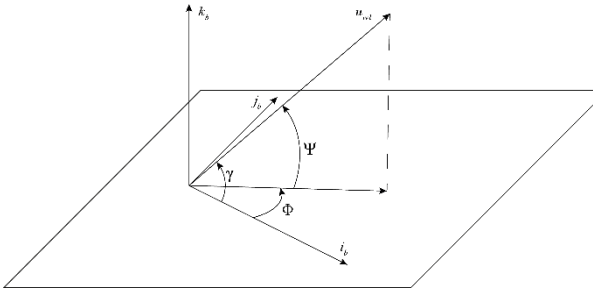

Fig. 4. Representation of the stability angles.

In addition, several numerical simulations have been carried out. In particular, a set of initial conditions in terms of orbital parameters (initial altitude, inclination and RAAN) have been analysed, to characterize those regions where the sail achieves its target performance. In addition, another feature of the initial orbit was strongly considered to mark different simulation results, i.e. the Earth shadowing effect. The latter has the result of introducing discontinuities in the external torque acting on the satellite, since the SRP has no effects when the CubeSat enters the Earth shadow region, leading to possible pointing loss. A further remark must be done in the distinction between "in light" and "shadowed" orbits: an orbit is considered "in light" if, propagating the two body problem equations without adding the perturbation term and fixing the Sun position, for an entire period, all the points of such orbit are not in Earth shadow. It means that during the simulation, when the perturbations and the motion of the Sun are included, the satellite can enter anyway the shadow region, after a certain number of orbital periods; in general, the higher the inclination is, the more this downside can be avoided.

The sensitivity analysis results for different initial orbit conditions are shown in Fig. 5 and Fig. 6. From the resulting maps it is possible to identify three different regions:

1. below 500 km of initial altitude the satellite arrives at 250 km without losing the desired pointing, almost independently from the inclination or RAAN (with few exceptions specifically for RAAN = 180 deg). This means that this region can be identified as the most suitable for a completely passive de-orbit.
2. above 525 km of initial altitude the simulation always fails, independently from the Earth shadow: this implies that the SRP effect is not negligible if compared with drag, so the desired pointing direction cannot be maintained passively.
3. between 500 km and 525 km of initial altitude the map does not show a defined pattern with the RAAN, the inclination or the altitude itself. This can be explained by the fact that the Earth shadow tends to increase the possibility of losing the pointing direction: since the SRP torque is "turned on" and "off", the equilibrium attitude position changes abruptly when the satellite enters and exits the shadow region, leading in some cases to greater oscillations and attitude loss. It is possible to notice that the "in light" orbits, in part highlighted with the red box in Fig. 5 and in part presented in Fig. 6, show a more regular trend with altitude, compared to the ones partially shadowed by the Earth. The white boxes for inclination greater than 70 deg come from the fact that at the related altitudes the Earth shadows part of the orbit.

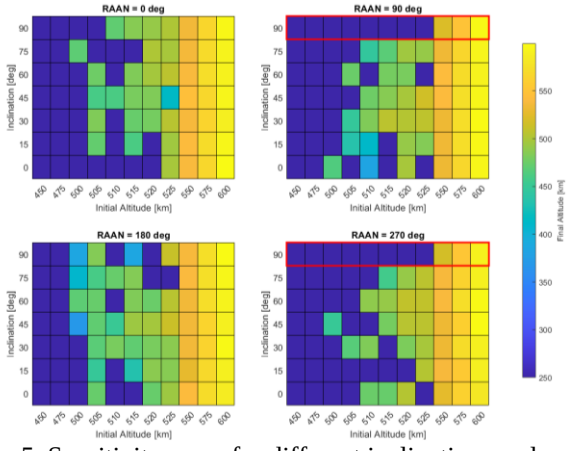

Fig. 5. Sensitivity maps for different inclinations and RAAN.

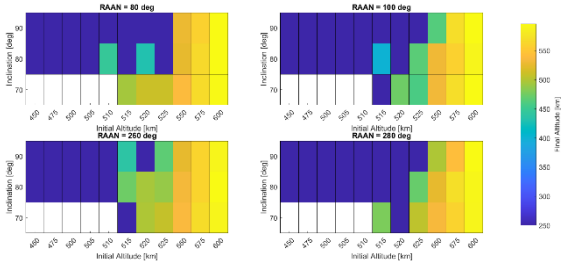

Fig. 6. Sensitivity maps for different inclinations and RAAN of "in light" initial orbits.

3.2.1 De-orbiting example

An example of a stable de-orbit is here presented. The nominal initial orbit chosen for the simulation is characterized by the following Keplerian parameters:

Table 1: Geometrical data used in simulations

a [km]	e [-]	inc [deg]	$RAAN$ [deg]	$\omega_{perigee}$ [deg]	θ [deg]
6871	0	0	0	0	0

Fig. 7 shows the trend of the altitude of the satellite with the time, demonstrating the effective de-orbiting: even if the orbit is partially shadowed by the Earth, the sail succeeds in its stabilizing effect.

Fig. 8 shows the behaviour of the stability angles, during the presented de-orbiting. It can be noticed that the out-of-plane angle Ψ is small only for few periods at the beginning of the simulation, but then the oscillations increase in magnitude: this means that the 2D approximation of the attitude motion assumed in many previous works [8] [9] is valid only for the first part of the de-orbiting. In addition, it is possible to identify a converging trend in the satellite oscillations indicated by the three angles after ≃ 400 periods, which correspond to an altitude of ≃ 350 km (see Fig. 7): this justifies the decision of interrupting the simulations when the CubeSat reaches 250 km of altitude, since below this height the sail stabilization effect is guaranteed.

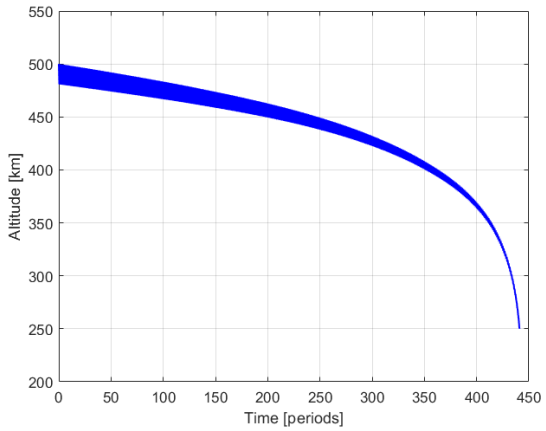

Fig. 7. Satellite altitude evolution in time.

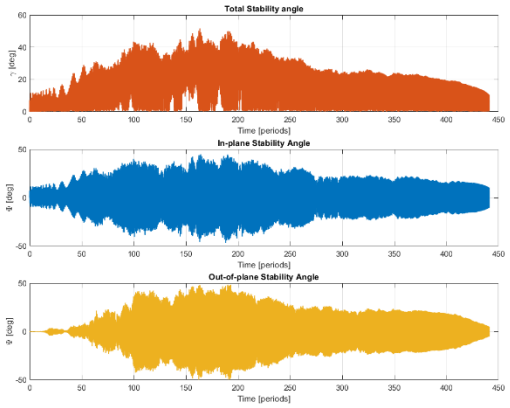

Fig. 8. Stability angles evolution in time.

4. Technology

In this section, a preliminary design of the drag sail module is described, with the aim of storing it in 1U. This modular drag sail is designed to provide minimum intrusion to the remaining CubeSat parts. A brief analysis of the deployment system is also presented: the final configuration is consistent with the sail geometry, so the booms are mounted to be deployed with the correct inclination. To prevent them from hitting the frame edges, a mechanism is selected to shift the central supporting panel to the level of the upper panel, avoiding any damage to the system.

4.1 Boom analysis

Great attention has been given to the booms study, which are very important for keeping the sail shape. The first step was to select a proper technique for their design: this analysis was done following the directions indicated in [10].

Inflatable structures folded with origami patterns were selected since they provide compactness of the folded components and an axial deployment. Among various origami techniques, the Miura folding was chosen since it is quite simple, it leaves more space for the sail storage, and it provides better straight-line deployment. Fig. 9 shows a single module of a Miura folded cylinder, composed by different layers of height H. Each layer is formed by n cells, each one is a trapezoid characterized by d_1, d_2, φ_1, φ_2, with a total length of $2\pi R$.

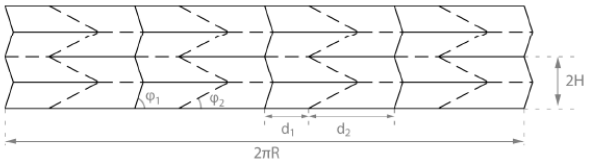

Fig. 9. Miura pattern.

Among the aforementioned parameters, the design variables are R, n, φ_1. After their selection, the dependant

parameters can be easily computed by means of mathematical formulations. The final configuration of the Miura-Ori cell pattern is reported in Tab. 2.

Table 2: Miura cell parameters

φ_1 [*deg*]	φ_2 [*deg*]	d_1 [*mm*]	d_2 [*mm*]	H [*mm*]
66	30	8.5	16.6	6.3

After the definition of the Miura-Ori cell parameters, a kinematic analysis has been performed, with the aim of using the half-module width H of the cylinder to study the mechanical behaviour of the deployable structure. The idea was to solve a system of nonlinear equations and to retrieve some unknown parameters at each width, from 0 to H. Then, for every step, the Miura-Ori cell points are evaluated by means of kinematic relations. The initial and final configurations are shown in Fig. 10.

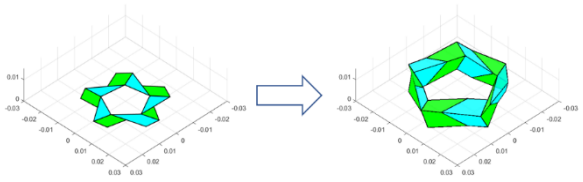

Fig. 10. Miura-Ori deployment kinematics.

During the overall de-orbit phase, the booms must remain rigid, hence the internal pressure is used to keep the booms inflated and rigid enough to have the sail well deployed. This concept is discussed in [11]: the boom is described as a thin wall cylindrical structure (membrane element) which exploits the pre-stress condition given by the internal pressure to withstand external loads and keep its shape. Regarding the material, a laminate composed of two 14.5 µm aluminium layers and a 16 µm of BoPET was selected.

4.2 Sail folding methods

Correctly folding the sail membrane will affect how the sail deploys and the sail efficiency. The most classic techniques are Z-folding and origami. An interesting alternative, known as square-twist method [12], can provide benefits in volume-constrained applications. Among the aforementioned methods, two alternatives were considered, again taken from [10], that are: modified square-twist method and double direction z-folding. Since the first increases the design complexity, the second was preferred. It consists in folding the sail first along one direction, then along a perpendicular one. At the end, the sail will be stored in a prismatic configuration: the first apex of the triangle will be attached to the central support, the other two edges to the booms. For what concerns the material, it consists of a 13 µm layer of Kapton (capable of withstanding high temperatures) with a 300 Å aluminium coating on both sides. The double z-folding procedure is shown in Fig. 11.

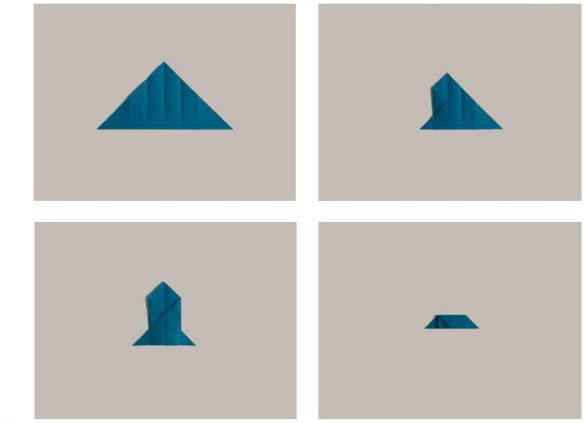

Fig. 11. Double z-folding.

4.3 Multi-objective optimization

A multi-objective optimization analysis has been implemented to retrieve the values of all the final configuration parameters. The selected design variables are:

L = length of the boom
R = radius of the boom
P = pressure in the inflated boom
Hc = distance from the upper panel to the booms support

To achieve correct results, each variable value is limited between an upper and a lower boundary, reducing the search domain. Then, their optimal values are selected to minimize the following objective functions:

1. Folded boom height $h_{effective}$
2. $1/K$, i.e tip displacement
3. $\Delta P/P$ with $\Delta P = P_{in} - P$
4. $1/R$
5. $1/L$

The final results are reported in Tab. 3

Table 3: Final parameters selected

P [*bar*]	L [*mm*]	R [*mm*]	H_e [*mm*]
1.3	1450	20	46

4.4 Final configuration

A preliminary system design is proposed to show that the drag sail module can be stored in 1U. The overall unit consists in the sail, the booms, tanks filled with pressurised gas, valve to command the boom deployment, a supporting structure and a deployment mechanism activated by the hold and release mechanism. In particular, the inflation system consists of four spherical tanks filled with nitrogen and a zero-leakage solenoid valve, selected to guarantee a proper pressure level inside the booms, therefore their rigidization. The mass of the main selected components (valve excluded),

along with the total mass, is reported in Tab. 4, while the internal configuration of the module is shown in Fig. 12.

Table 4: Components mass (all values in [*kg*]

Frame	Tank	Support	Booms	Sail	Total
0.133	0.069	0.152	0.08	0.095	0.520

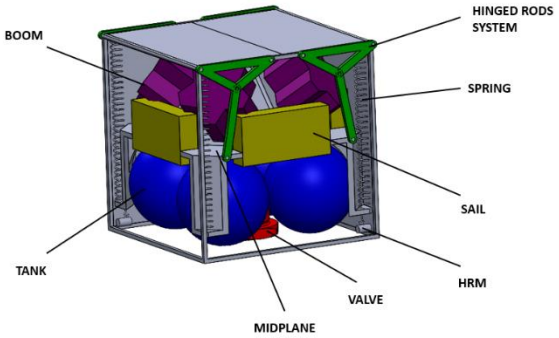

Fig. 12. View of the internal configuration of the drag sail module.

The deployment is obtained in two steps:

1. **Mid plane motion**. If the booms were directly deployed from the stored configuration, they would hit the frame edges. For this reason, the central plane should be moved upwards replacing the upper surface, which is composed by two panels. A simple hold and release mechanism, which consists in small resistors linked with a nylon wire, forces the midplane to stay in the predefined position, pre-stretching the springs. When the resistors heat up, the wire is cut and the midplane is released. The two upper panels can open consequently. For the latter, two solutions are proposed:
   a) a resistors-wire system, equal to the one used to keep the midplane in place;
   b) a simple mechanism composed of rods hinged to the midplane and the upper panels.

   Once the midplane reaches the top, the booms can be inflated and deployed. Figs. 13a to 13c illustrate the process described above, considering the hinged rods solution.
2. **Inflation with gas**. When exposed to space, the booms will be deployed. However, if the ΔP between the stored gas and the outside is too high the inflation process could tear the booms. The solution proposed is to leave a small amount of gas inside the boom support, stored at low pressure, so the first step of the inflation process will be slow enough. Then, by means of a solenoid valve, at each step a small mass of gas will flow from the tanks to the booms, until the gas pressure equals the nominal one.

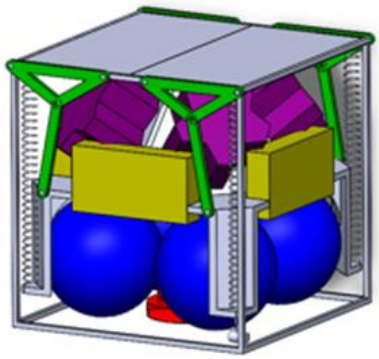

(a) Closed configuration

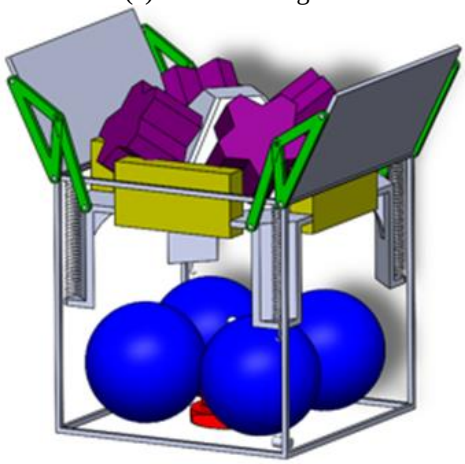

(b) Intermediate opening step

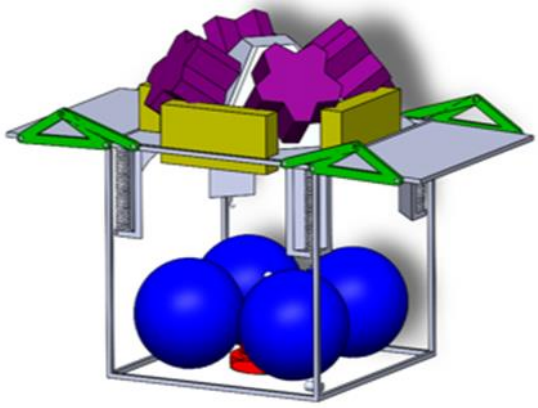

(c) Opened configuration

Fig. 13. Opening steps.

5. Manufacture

This section is devoted to the description of a possible manufacturing process. For what concern the booms, the limited diameter precludes to manually support the material from the inside, to correctly fold the structures. A novel manufacturing method was developed and reported in [13]:

1. The aluminium-laminate is wrapped around a cylindrical mandrel;

2. A stiff plastic sheet, previously folded with the correct pattern, is wrapped around the pressurized boom;
3. The pressure inside the boom is used to press the laminate material against the plastic mandrel;
4. The plastic is removed, and the boom compressed in its stowed dimensions.

Instead, regarding the drag sail manufacturing process [14], it is quite common to use plastic or paper guides with holes. An alternative could be the use of local stiffness variations: when the material is folded and unfolded, it is easy to refold it along the same lines because it has been plastically deformed. A third method is the use of a channel (as a plastic strip) to drive the folding process. Since the sail folding process is easier if compared to the booms one, it has been actually implemented. A material with thickness and properties similar to the original Aluminium-Kapton layer has been employed and folded with the help of plastic strips. The main steps of the folding process are shown in Figs. 14a to 14d.

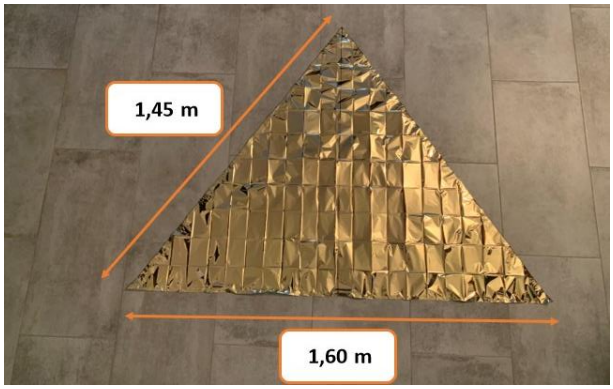

(a) Unfolded Sail

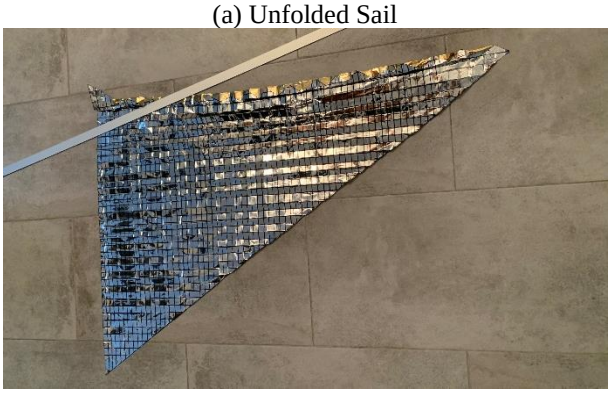

(b) First folding step

(c) Second folding step

(d) Folded Sail

Fig. 14. Sail folding steps.

The implementation, although rudimentary and done manually, has nevertheless shown encouraging results which can be improved using more sophisticated equipment. The comparison between the theoretical and experimental dimensions of the folded sail are shown in Fig. 15

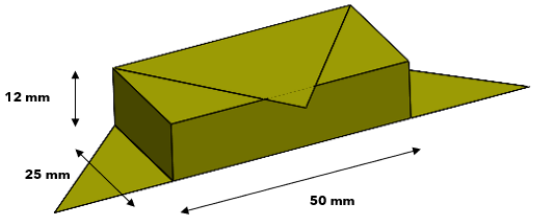

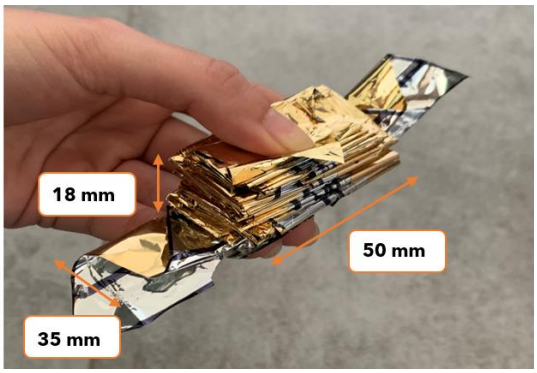

Fig. 15. Folded sail dimensions.

6. Conclusions

This work was meant to evaluate the stabilization effect of a pyramid-shaped sail in terms of attitude dynamics and to find a technical solution to store the drag sail module in 1U CubeSat. A dynamic model was implemented to study the evolution of the satellite during the de-orbiting phase. The model was used to test several initial conditions in terms of orbital parameters, understanding the limits of the pyramidal sail as a passive attitude stabilization device. These simulations have shown that, in the drag dominated region, stability can be maintained while some issues arise in the region where drag and SRP become comparable, and the presence of eclipses favours the satellite tumbling.

Then, a design process was performed, leading to the selection of inflatable structures folded with Miura-Ori pattern as booms, due to the compact stored

configuration and the straight-line deployment. To keep the sail correctly deployed, the booms need to be maintained rigid, so a pressurizing system was designed. Concerning the sail, the double z-folding technique was preferred as it ensures ease of manufacturing and compactness. Then, the design parameters of the final configuration were selected through a multi-objective optimization process, implemented to test several combinations, and determine the most suitable one.

Future studies shall focus on refining the system design: in particular, a more detailed thermal and structural analysis should be performed, further tests should assess if the module components can be effectively realized with the proposed dimensions, or they should be adjusted to fit 1U.

References

[1] M. Yakovlev. The "IADC space debris mitigation guidelines" and supporting documents. In 4th European Conference on Space Debris, volume 587, pages 591–597. ESA Publications Division Noordwijk, The Netherlands, 2005.

[2] B. Fu, E. Sperber, F. Eke. Solar sail technology—a state of the art review. Progress in Aerospace Sciences, 86:1–19, 2016.

[3] W.K. Belvin, M. Straubel, W.K. Wilkie, M. Zander, J.M. Fernandez, M. Hillebrandt. Advanced deployable structural systems for small satellites. 2016.

[4] M. Schenk, A.D. Viquerat, K.A. Seffen, S.D. Guest. Review of inflatable booms for deployable space structures: packing and rigidization. Journal of Spacecraft and Rockets, 51(3):762–778, 2014.

[5] D.A. Vallado. Fundamentals of Astrodynamics and Applications. Springer Science & Business Media, 2001.

[6] H.D. Curtis. Orbital Mechanics for Engineering Students. Elsevier, 2010.

[7] F. L. Markley, J.L. Crassidis. Fundamentals of Spacecraft Attitude Determination and Control. Springer, 2014.

[8] N. Miguel Banos, C. Colombo. Deorbiting spacecraft with passively stabilised attitude using a simplified quasi-rhombic-pyramid sail. Advances in Space Research, 67(9):2561–2576, 2021.

[9] N. Miguel Banos, C. Colombo. Stable attitude deorbiting using a simplified planar quasirhombic-pyramid sail. In 5th International Symposium on Solar Sailing, pages 1–13, 2019.

[10] C. Giovannini. Solar sail strategies for satellite's direct and modulating deorbiting. 2021. http://hdl.handle.net/10589/183320

[11] A. Zanelli, C. Monticelli, M. Mollaert, B. Stimpfle. Inflatable beams subjected to axial forces. 2019.

[12] C. Mason, G. Tilton, N. Vazirani, J. Spinazola, D. Guglielmo, S. Robinson, R. Bevilacqua, J. Samuel. Origami-based drag sail for cubesat propellant-free maneuvering. In 5th Nano-Satellite Symposium, 2013.

[13] Inflatesail. (Accessed 09-02-2022) https://directory.eoportal.org/web/eoportal/satellite-missions/i/inflatesail

[14] O.R. Stohlman, J.M. Fernandez, G. Dean, N. Schneider, J. Ho Kang, R. Barfield, T. Herndon, P. Stokes. Advances in low-cost manufacturing and folding of solar sail membranes. In AIAA Scitech 2020 Forum, page 2167, 2020.